Self-Assembling All-Enzyme Hydrogels for Compartmentalised Biocatalysis

Theo Peschke[1], Sabrina Gallus[1], Patrick Bitterwolf[1], Yong Hu[1], Claude Oelschlaeger[2], Norbert Willenbacher[2], Kersten S. Rabe[1] and Christof M. Niemeyer[1*]

Supplementary Information

Contents

[1] Institute for Biological Interfaces (IBG 1), Karlsruhe Institute of Technology (KIT), Hermann-von-Helmholtz-Platz 1, 76344 Eggenstein-Leopolshafen, Germany. [2]Institute Mechanical Process Engineering and Mechanics, Karlsruhe Institute of Technology (KIT), Gotthard-Franz-Straße 3, 76131 Karlsruhe, Germany. Correspondence and requests for materials should be addressed to C.N. (email: niemeyer@kit.edu).

Materials and Methods

Plasmid construction. The plasmid for the soluble protein Gre2p-His[1] was a previously described expression vector. Unless otherwise stated, the genetic construction was carried out using the isothermal recombination as described by Gibson et al.[2] utilizing oligonucleotide primers with 30 bp homologous overlaps. After the assembly, the reaction mixtures were treated with DpnI to remove any remaining vector from prior PCR reactions and then transformed into *E. coli* DH5α cells. All plasmids were purified using ZR Plasmid Miniprep–Classic (Zymo Research, Germany) according to the manufacturer's instructions and sequence verified by commercial sequencing (LGC genomics, Germany). The plasmid encoding for P450 BM3 (A74G, F87V)-His was generated in two steps, based on the previously described plasmid pEXPn28_BM3-A74G-F87A[3] with a c-terminal HOB- and His-Tag. In a first step, P450 BM3 F87A was converted to F87V by utilizing the primers KSR168 (CGTGATTTTGCAGGAGACGGGTTAGTTAC) and KSR169 (GTCTCCTGCAAAATCACGTACAAATTTAAGACCTTG). Subsequently, the HOB-Tag was removed by amplification of the plasmid using the primers TB19 (GTGTGGGCTGGGAGCGGCGGTCATCATCACCATCAC) and TB20 (CCCAGCCCACACGTCTTTTGCGT). The backbone encoding for a c-terminal HisTag separated by a glycine spacer used for generating pET_GDH-His was amplified utilizing primers SG10 (ATGTATATCTCCTTCTTAGTACAAACTTG) and SG25 (GGTCATCATCACCATCACCATTGAG) with pET_Gre2p-ST-His[4] as the template. This backbone was then recombined with a GDH encoding insert, which had been generated by PCR using the primers SG23 (ACAAGTTTGTACTAAGAAGGAGATATACATATGTATCCGGATTTAAAAGGAAAAGTCG) and SG26 (TCAAACTCAATGGTGATGGTGATGATGACCACCGCGTCCTGCCTGGAAAG) with pEXPn15_GDH-SBP as the backbone[4]. Similar, pET_Gre2p-ST-His was used as a template for a PCR with the primers SG9 (GGTGGTGGTGGTAGCGCC) and SG10 resulting in a backbone encoding for a c-terminal GGGGS-ST-G-His. The insert encoding for GDH with a c-terminal GGGGS-Linker was amplified with the oligonucleotide primers SG23 and SG24 (CAATATGGGCGCTACCACCACCACCGCTACCACCACCACCACCGCGTCCTGCCTGGAAAG) using pEXPn15_GDH-SBP as the template. A GGGGS-linker sequence was introduced by overlaps in the SG24 primer. The final pET_GDH-$(GGGGS)_2$-ST-G-His plasmid was obtained by Gibson assembly of the insert sequence encoding for GDH-GGGGS and the backbone encoding for GGGGS-ST-G-His. To generate the plasmid pET_His-G-ST-eGFP-His, the His-Tag and a glycine spacer were inserted into pET_ST-eGFP-His plasmid[5] by PCR using the primers TP25 (ATGATGGTGGTGATGATGCATGTATATCTCCTTCTTAAAGTTAAACAAAATTATTTC) and TP26 (CATCATCACCACCATCATGCACATATTGTTATGGTTGATGCCTATAAACCG). The pET_His-LbADH plasmid was constructed by Gibson assembly of an LbADH insert, prepared by PCR with the primers SG31 (ATATACATGCATCATCACCACCATCATGGTAGCAATCGCCTGGATGGTAAAGTTG) and SG32 (CTTTCGGGCTTTGTTAGCAGCCGGATCTTACTGTGCGGTATAACCACCATCC) with pEXPn3_His-LbADH[5] as the template and a backbone amplified with SG05 (TAAGATCCGGCTGCTAACAAAGCC) and SG30 (ACCATGATGGTGGTGATGATGCATGTATATC) with pET_His-G-ST-eGFP-His as the template. Generation of pET_His-SC-GGGGS-LbADH was achieved by recombination of two different inserts: The first insert encoding for the LbADH was amplified with the primers SG32 and SG33 (GGTGATGCACATATTGGTGGTGGTGGTAGCAGCAATCGCCTGGATGGTAAAGTTG) with pEXPn3_His-LbADH as the template, and the second insert encoding for SC-GGGGS was generated by PCR with the primers SG34 (ATATACATGCATCATCACCACCATCATGGTGTTGATACCCTGAGCGGTCTG) and 35 (GCTACCACCACCACCAATATGTGCATCACCTTTGGTTGC) and pTF16_ompA-SC [5] as the template. The GGGGS spacer sequence was introduced using the primer SG34. Both inserts were recombined in a one-pot reaction with the backbone amplified with SG05 and SG30 and pET_His-G-ST-eGFP-His as the template.

Expression and purification of proteins. For heterologous protein expression, *E. coli* BL21 (DE3) was transformed with the corresponding expression vector using heat shock transformation. The freshly transformed *E. coli* cells harboring the various plasmids were selected overnight on LB/agar plates containing 100 µg/ml ampicillin at 37°C. Liquid cultures of 160 ml LB medium containing ampicillin were generated from clones of the LB/agar plates cultured overnight for 14-18h at 37 °C, 180 rpm in a 500 ml shaking flask. 2 L ampicillin containing LB-medium was inoculated 1:20 with overnight culture. The cultures were incubated at 37°C, 180 rpm until an OD_{600} of 0.6. The temperature was then lowered to 25°C, IPTG was added to a final concentration of 0.1 mM and the cultures were incubated for an additional 16 hours. The cultures were pooled and cells were harvested by centrifugation (10000xg, 10 min) and resuspended in 60 mL buffer A (50 mM NaH_2PO_4, 300 mM NaCl, 10 mM Imidazole, pH 8.0). After disruption by ultrasonication, the cell lysate was obtained after centrifugation (45000xg, 1 h), filtered through a 0.45 µm Durapore PVDF membrane (Steriflip, Millipore) and loaded on two HisTrap FF (5 mL) Ni-NTA columns (GE Healthcare, Germany) connected in series and mounted on an Äkta Pure liquid chromatography system (GE Healthcare, Germany). The column was washed with 100 mL buffer A and the 6xHis-tagged proteins were eluted using a gradient from 100% buffer A to 100% buffer B (50 mM NaH_2PO_4, 300 mM NaCl, 500 mM Imidazole, pH 8.0) over a volume of 200 ml. Subsequently, the buffer was exchanged to KP_i-Mg using Vivaspin 10 000 MWCO (GE Healthcare).

To characterise the recombinant, purified proteins, samples were typically analyzed by standard discontinuous SDS-polyacrylamide Laemmli-midi-gels. The bands were visualized by Coomassie staining and were compared to the Color Prestained Protein Standard, Broad Range (New England Biolabs). The concentrations were determined by UV-Vis spectroscopy, using the theoretical molar extinction coefficients at 280 nm, as calculated by the Geneious version 9.1.3 software[6].

Dynamic light scattering (DLS). Time-dependent increase of hydrodynamic diameter upon polymerisation was determined by dynamic light scattering (DLS) using the Nano-Series ZetaSizer (Zetasizer Nano ZSP, Malvern Instruments), equipped with a He-Ne-Laser (633 nm). Before the measurement, all protein solutions were preincubated in a thermoshaker for 5 minutes at the temperature of the following measurement and 500 rpm. Subsequently, if not stated otherwise, two 50 µl protein solutions (100 µM) were mixed in a UV-cuvette at a molar ratio of 1:1. The parameters of this experiment were varied in terms of different temperatures, protein concentrations or stoichiometry. The average hydrodynamic radius of the protein particles (Z-Average), calculated from auto-correlated light intensity data using the ZetaSizer Software, was recorded over 2 hours with individual measurements every 90 s. The increase of the average hydrodynamic radius within the first 30 min of SC-ST polymerisation was calculated and used for comparison of the influence of the various parameters on the hydrogelation.

Multiple particle tracking (MPT) based optical microrheology. Prior to MPT-analysis, the dried hydrogel samples were swollen by adding 10 µl KP_i-Mg for 10 minutes under continuous shaking at 25°C, 500 rpm. MPT experiments were performed using an inverted fluorescence microscope (Axio Observer D1, Zeiss), equipped with a Fluar 100x, N.A. 1.3, oil-immersion lens combined with a 1x optovar magnification changer. The Brownian motion of more than 100 green fluorescent polystyrene microspheres of 200 nm diameter used as tracer particles was tracked. Images of these fluorescent beads were recorded using a sCMOS camera Zyla X (Andor Technology, UK). Displacements of particle centers were monitored in an 127 x 127 µm field of view, at a rate of 50 frames/s. Movies of the fluctuating microspheres were analyzed using a custom MPT routine incorporated into the software Image Processing System (Visiometrics iPS) and a self-written Matlab program[1] based on the widely used Crocker and Grier tracking algorithm[7].
To characterize sample heterogeneities, we analyzed the distribution and slopes of the MSDs. We further calculated the van Hove correlation functions[8], i.e., the probability distribution of particle displacement for an ensemble of N tracked particles as:

$$P(x,\tau) = \frac{1}{N}\left\langle \sum_{i=1}^{N} \delta[x + x_i(0) - x_i(\tau)] \right\rangle = \frac{N(x,\tau)}{N}$$

Where $N(x,\tau)$ is the number of particles found at positions between x and x + dx along the x-coordinate. $P(x,\tau)$ is Gaussian if all tracer particles are exposed to a similar environment. Deviations from this functional form reflect the presence of spatial heterogeneities and can be characterized by the non-Gaussian parameter α [9].

$$\alpha = \frac{\langle x^4(\tau)\rangle}{3\langle x^2(\tau)\rangle^2} - 1$$

This quantity is zero for a Gaussian distribution, while deviations can result in large α values.

Scanning electron microscopy (SEM). The hydrogel was swollen for at least 10 minutes at RT by adding 20 µl KP_i-Mg and subsequently mounted on SEM target grids. SEM images were obtained using a QUANTA 650-FEG scanning electronmicroscope (FEI Company, USA) with an accelerating voltage of 5-10 kV.

Atomic force microscopy (AFM). Prior to AFM analysis, the dried hydrogel sample was swollen for 10 minutes by adding 20 µl KP_i-Mg-buffer. Subsequently a piece of the gel with an approximate volume of 25 µl was deposited on freshly cleaved mica surface (Plano GmbH), allowed to adsorb for 3 min at room temperature and was then overlaid with 5 µl TEMg (20 mM Tris base, 1 mM EDTA, 12.5 mM, $MgCl_2$, pH 7.6 adjusted with HCl). The hydrogel was scanned in its swollen form with a MultiModeTM 8 microscope (Bruker) equipped with a Nanoscope V controller. A silicon tip on nitride lever cantilevers with sharpened pyramidal tips (ScanAsyst-Fluid+ tips 0.7 N/m, Bruker) was used and operated in the ScanAsyst mode. The images obtained were analyzed and processed by using the NanoScope Analysis 1.40 software.

Chip fabrication. The microfluidic chip design was previously described in detail[10]. In brief, the chip designs were based on the dimension of standard microscope slides (76 x 26 mm² DIN ISO 8037-1:2003-05). The upper part containing the reaction channel was manufactured by replica casting of polydimethylsiloxane (PDMS) (Sylgard 184, Dow Corning, USA) in brass replication molds. The straight channel was 3 mm wide, 1 mm high and 54 mm long with a total volume of 150 µL. Cannulas (Sterican, B. Braun Melsungen AG, Germany), were inserted through horizontal holes in the molds before pouring the PDMS prepolymer to serve as placeholders for the cannulas. The PDMS was cured at 60 °C for at least 3 h.

Chiral HPLC analysis. The synthesis and the characterization of NDK-**1** as well as the analysis of biocatalytic reaction products by chiral HPLC were performed as previously described[1]. In brief, the dried ethyl acetate extractions from the crude reaction mixtures (described above) were resuspended in 100 µl of the mobile phase (90% n-heptan, 10% 2-propanol) and 30 µl of that solution were injected into the HPLC instrument (Agilent 1260 series HPLC equipped with a Diode Array Detector (210 nm) and a Lux 3µ Cellulose-1 (150x2.00 mm) chiral column (Phenomenex). The hydroxyketones **2** were analyzed using method A (chromatography solvent 90% n-heptan/ 10% 2-propanol, 10 min isocratic, column oven temperature of 10 °C and a flowrate of 0.5 ml/min) and diols **3** by method B (chromatography solvent 98% n-heptan/ 2% 2-propanol, 20 min isocratic, column oven temperature of 45 °C and a flowrate of 1.0 ml/min).

Supplementary Figures

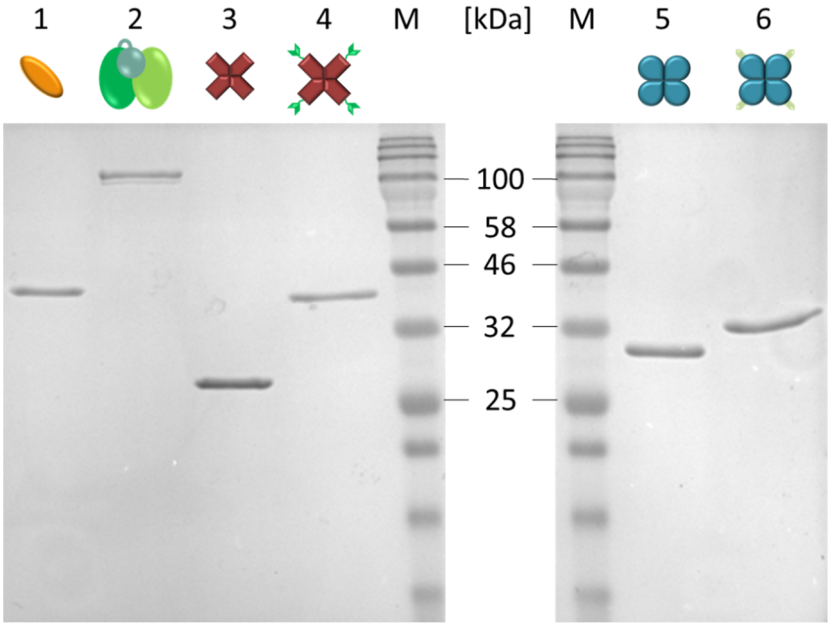

Supplementary Figure 1 | Molecular characterization of the enzymes used in this study. This is a 15% Coomassie stained SDS-PAGE. M: Color Prestained Protein Standard, Broad Range (New England Biolabs); lane 1: Gre2p-His (43 kDa); lane 2: P450 BM3 (A74G, F87V)-His (119 kDa); lane 3: His-LbADH (27 kDa); lane 4: His-SC-LbADH (40 kDa); lane 5: GDH-His (29 kDa); lane 6: GDH-ST-His (31 kDa).

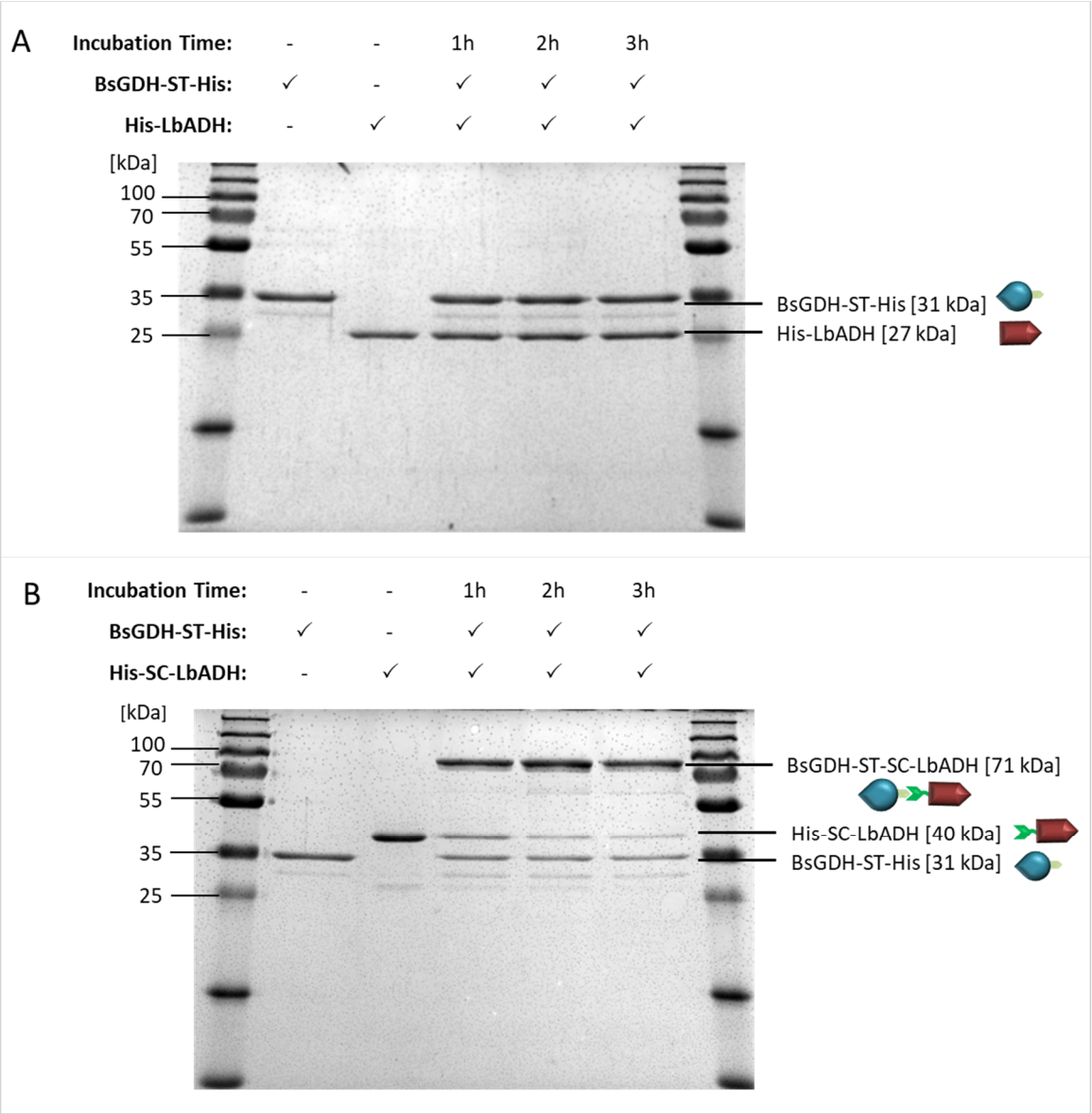

Supplementary Figure 2 | ST/SC-conjugation activity of GDH-ST and SC-LbADH analysed by Coomassie stained 15 % SDS-PAGE. Stoichiometric amounts (35 pmol) of both enzymes were incubated for up to 3 hours at 30°C and 1000 rpm. The reaction was stopped by addition of SDS-loading dye and incubation at 95°C for 10 minutes to denature non-covalent protein interactions. (**A**) As expected, the GDH-ST-His (31 kDa) does not react with the His-LbADH (27 kDa). (**B**) As expected, the GDH-ST-His (31 kDa) covalently links with the His-SC-LbADH (27 kDa) to form GDH-ST-SC-LbADH (71 kDa). Grayscale analysis revealed a coupling rate of the GDH-ST monomers with the SC-LbADH monomers of 85% after 3 hours. The non quantitative coupling is in agreement with previous publications[11, 12].

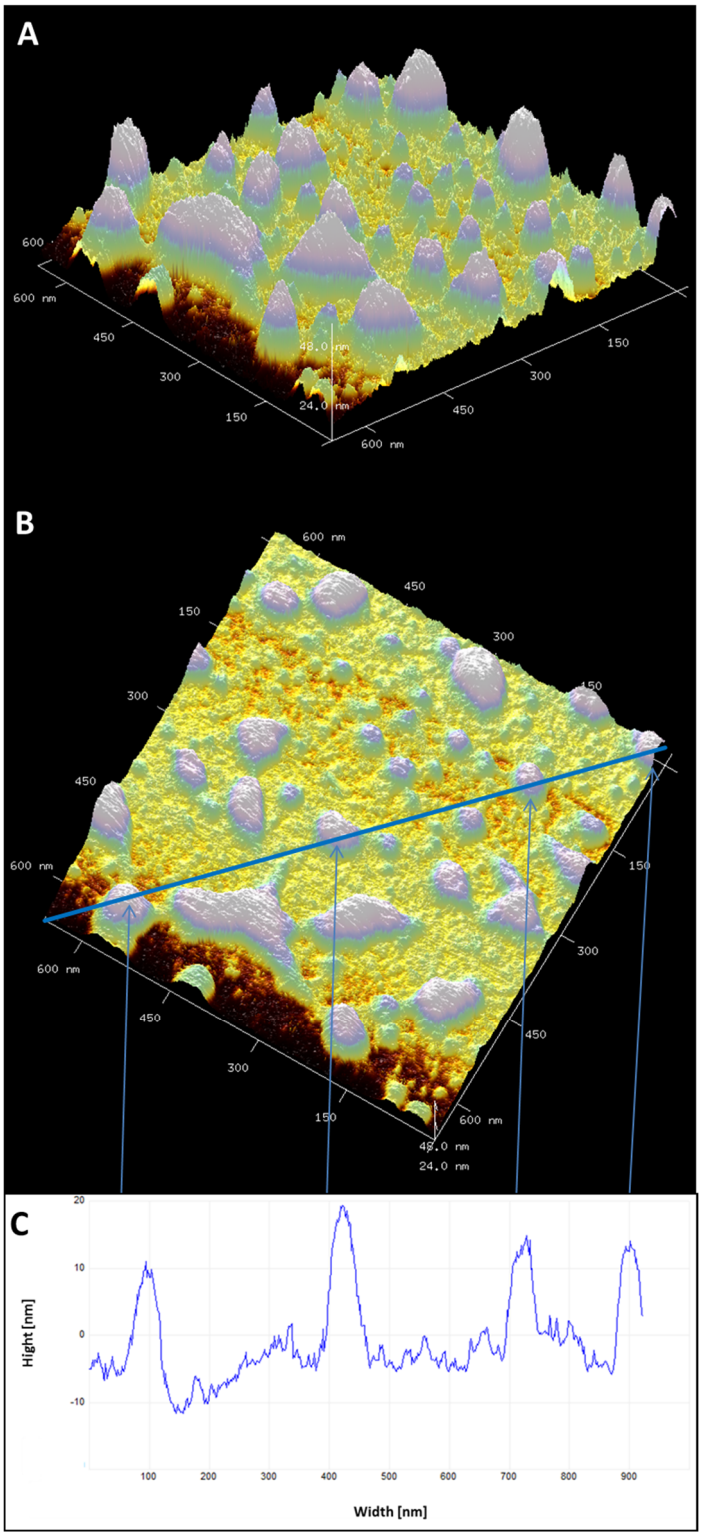

Supplementary Figure 3 | Analysis of surface topography of the swollen hydrogel by atomic force microscopy (AFM). Side view **(A)** and top view (**B**) of a 3D representation obtained by AFM. (**C**) Cross section analysis, as indicated by the blue line in (**B**), suggests a hydrogel structure consisting of a network of interconnected particles with an average particle size of approximately 50 nm. The exemplary Root Mean Square (RMS) roughness of this section was 3.14 nm.

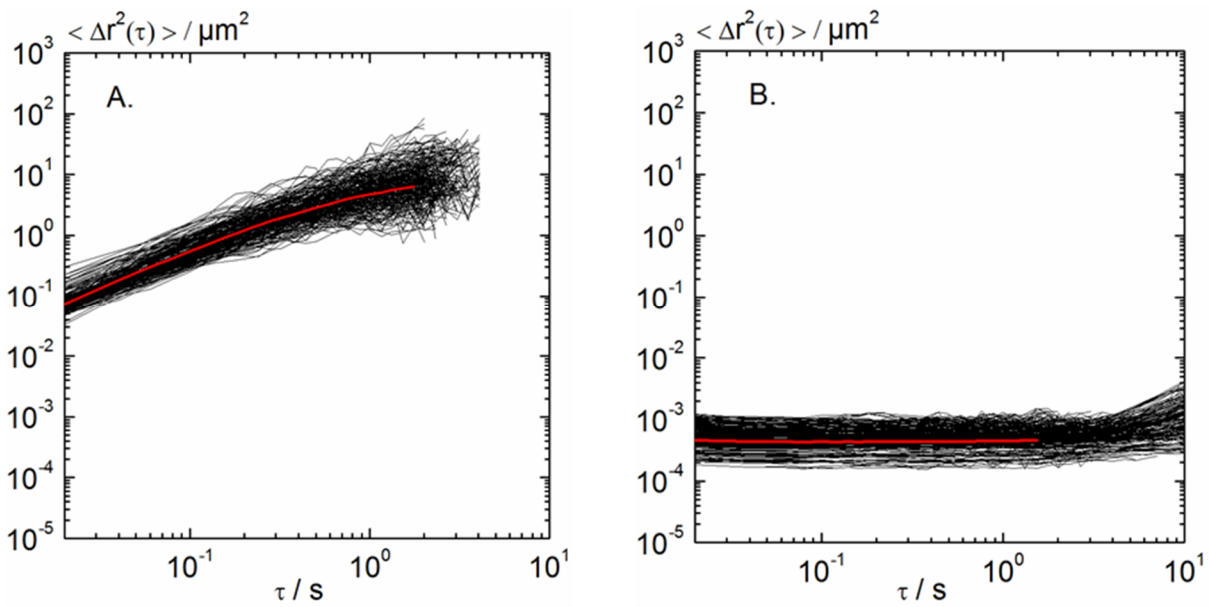

Supplementary Figure 4 | Analysis of the viscosity of the hydrogel using Multiple Particle Tracking (MPT) analysis in comparison with non-polymerized control enzymes. Mean square displacements (MSDs) of individual polystyrene microspheres of diameter 200 nm dispersed in a solution containing the soluble enzymes (**A**) or the hydrogelated enzymes (**B**). The red curve is the ensemble-average MSD. For measurements performed with the soluble enzymes (**A**), MSDs traces adopt a power-law behavior as a function of time with a slope β close to 1 throughout the probed time scales, where β is given by the relation $\langle \Delta r^2(\tau) \rangle \sim \tau^{\beta}$. This result indicates that the motion of the beads is purely diffusive and that the microenvironment surrounding the particles responds like a viscous liquid. The apparent viscosity η_{app} was determined from the average MSD trace using the relation $\langle \Delta\, r^2(\tau) \rangle = 4D\tau$ in combination with the Stokes-Einstein relation $D = k_B T / 6\pi\eta a$, where *D* is the diffusion coefficient and *a* is the tracer particle radius. We found η_{app} = 1.55±0.22 mPa*s and this value is in good agreement with the viscosity of pure water. Additionally, statistical analyses of the MSD distribution clearly reveals a homogeneous structure on the micrometer length scale with a small value of the non-Gaussian parameter α≈1.

In the hydrogel (**B**), tracer particle motion is significantly different from diffusion in the soluble enzymes. In latter case, all MSDs exhibit almost no time dependence (β ≈ 0) with a narrow distribution of absolute values (α=0.5) and an average MSD value of Δr^2~4.7*10^{-4}±1.5*10^{-4} μm^2. This result indicates that tracer particles are highly constrained by the surrounding fluid, which is consistent with an elastic trapping of tracer particles in a homogeneous gel-like network. From the time-independent MSD value the elastic shear modulus G_0 can be calculated as $G_0 = 2k_B T / 3\pi a \Delta r^2$. We found $G_0 = 20{\pm}7\ Pa$ and from this latter value, we can directly determine the mesh size ξ of the network according to the classical theory of rubber elasticity[6] with $G_0 = \frac{k_B T}{\xi^3}$ and found $\xi = 60{\pm}7$ nm. This value is much smaller than the diameter of the embedded tracer particles (200 nm) and characterizes therefore the elastic properties and network structure in the vicinity of the corresponding tracer particles.

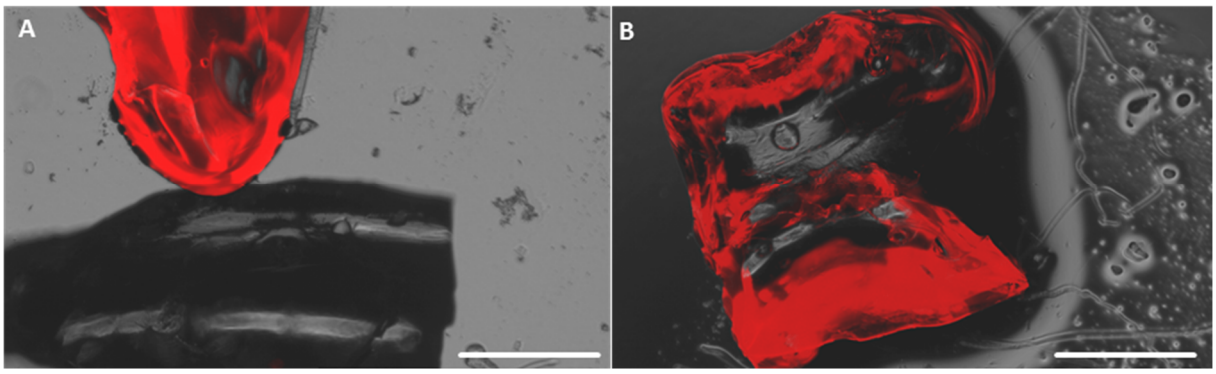

Supplementary Figure 5 | GDH-ST/SC-LbADH hydrogels reveal a dynamic morphology. Two pre-swollen hydrogel pieces (**A**), one labeled with fluorescent SYBR Orange Protein Gel Stain, were placed above one another and incubated in 20 µl KP_i-Mg buffer for 2 h (**B**). Note that the dye rapidly diffused into the unstained gel piece. Scale bars are 1 mm.

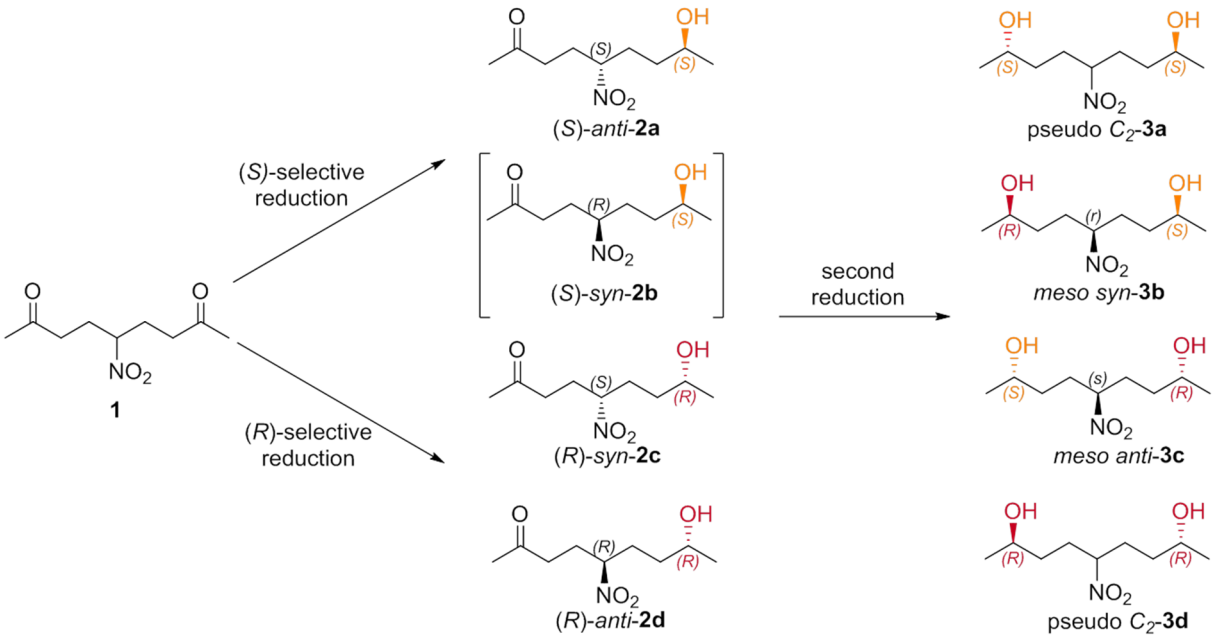

Supplementary Figure 6 | Reaction scheme of the reduction of NDK-1. The prochiral C_S-symmetrical 5-nitrononane-2,8-dione (NDK) **1** can be reduced, depending on the enzyme selectivity, either on one or on both of the two carbonyl groups to create the hydroxyketones **2** or diols **3**, respectively. All stereoisomers can be identified using by chiral HPLC. Please note that the (*S*)-*syn* hydroxyketone **2b** (in brackets) is not formed by the (*S*)-selective Gre2p due to the enzyme's extraordinary high *anti*-selectivity towards the 5-nitro-1-keto moiety of NDK-**1**[1].

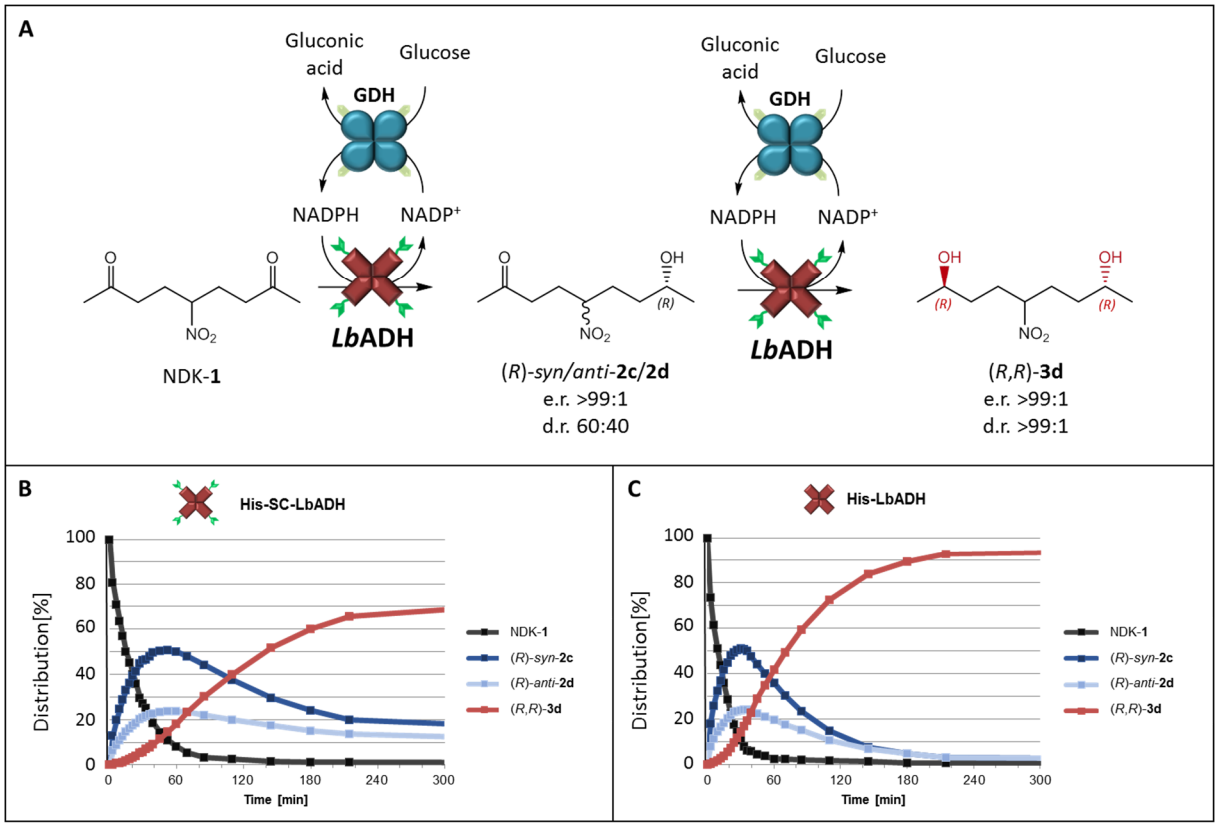

Supplementary Figure 7 | Time dependent stereoselective conversion of NDK-1 by the (*R*)-selective LbADH. (**A**) Reaction scheme of the conversion of NKD-**1** including the NADP(H)-regeneration by glucose-converting GDH. A reaction mixture containing the substrates NDK-**1,** glucose and the enzymes LbADH as well as an excess of GDH for cofactor regeneration was incubated at 30°C and samples were taken at defined time points and analyzed by chiral HPLC. (**B**) Product formation upon reactions employing His-SC-LbADH and (**C**) His-LbADH showing the (*R)*-selective conversion of NDK-**1** (black) to (*R*)-*syn*/*anti*-**2c/d** hydroxyketone (blue) which is directly reduced to (*R*,*R*)-configured pseudo C_2-**3d** (red).

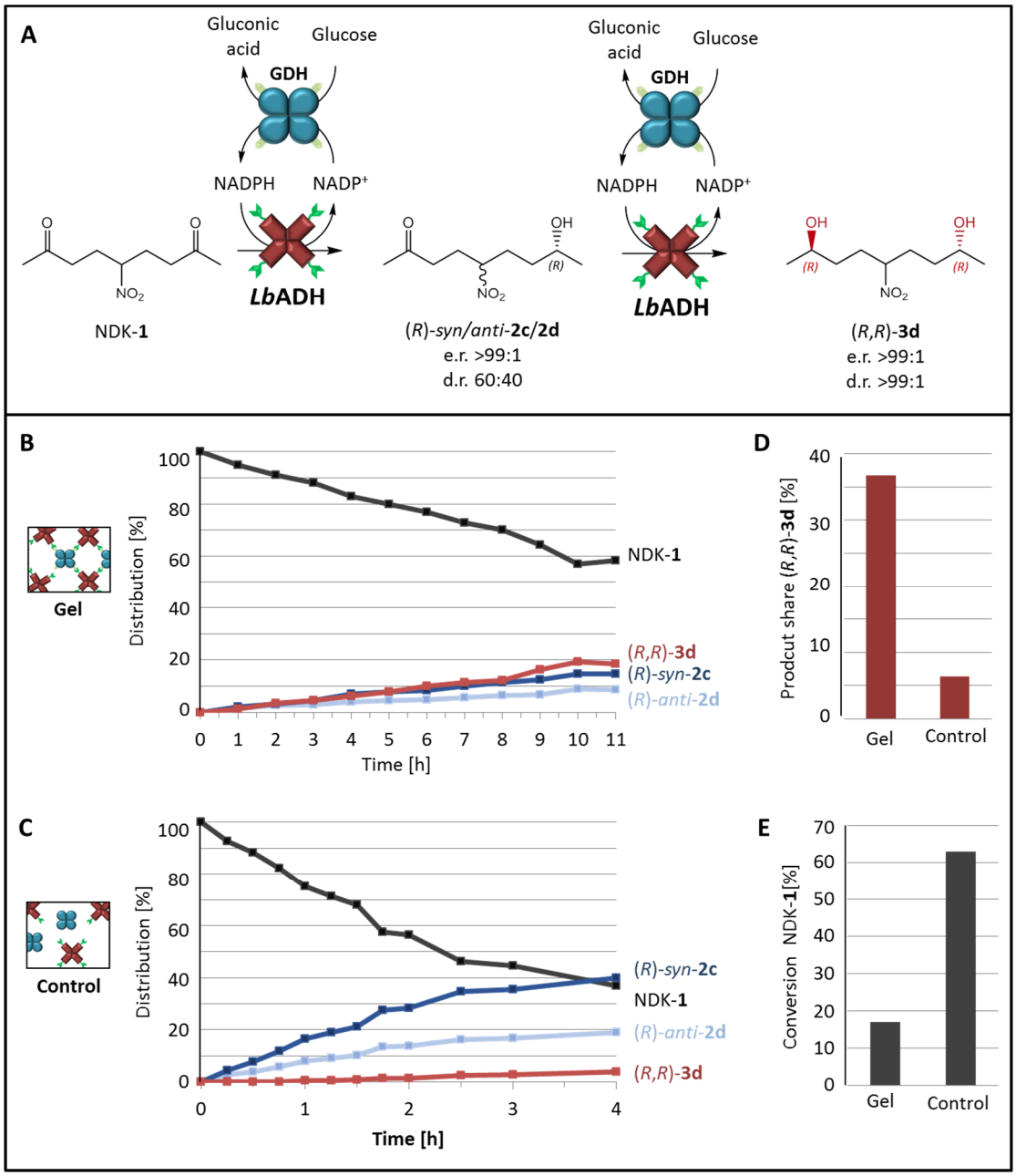

Supplementary Figure 8 | Kinetics of NDK-1 reduction employing the GDH-ST/SC-LbADH hydrogel or unassembled enzymes. (**A**) Reaction scheme and the corresponding reaction kinetics of (**B**) the hydrogel and (**C**) the unassembled GDH and LbADH-SC enzymes are showing the (*R*)-selective conversion of NDK-**1** (black) to (*R*)-syn/anti-**2c/d** hydroxyketone (blue) which is directly reduced to (*R*,*R*)-configured pseudo C_2-**3d** (red). Note that with the hydrogel, almost no formation of hydroxyketones was detectable. This indicates that NDK-**1** is directly reduced to diol-**3d**, whereas unassembled enzymes predominantly form the hydroxyketones instead of the diol, as indicated in (**D**), showing the percentage of diol-**3d** of all reaction products. The hydrogel reaction resulted in 37% of (*R*,*R*)-**3d** diol formation after 4 hours, while only 6% of (*R*,*R*)-**3d** was produced by the unassembled enzymes. (**E**) Conversion of NDK-**1** after 4 hours of reaction. Note that the hydrogel reveals a lower (17%) conversion than the unassembled enzymes (63%).

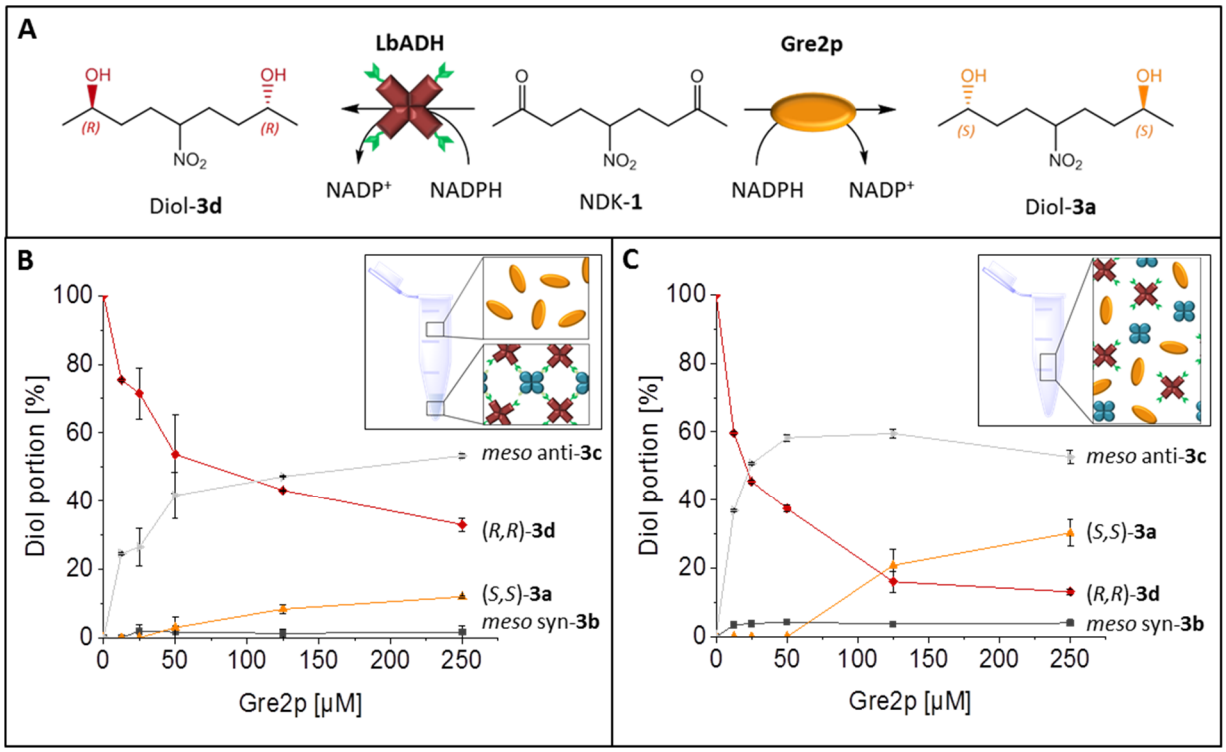

Supplementary Figure 9 | Two enzymes competing for the same substrate (NDK-1) and intermediates (hydroxyketones/NADPH) - Production of diols by GDH-ST/SC-LbADH (50 µM subunits, each) gels and variable concentrations of Gre2p in the compartmentalised competition assay (see Figure 2). (**A**) Simplified reaction scheme of the competitive assay between the (*R*)-selective ketoreductase LbADH converting NDK-**1** in a two-step reduction to (*R,R*)-configured diol-**3d** and the (*S*)-selective Gre2p converting NDK-**1** in two reduction steps to (*S,S*)-configured diol-**3a**. Note that the formation of the *meso*-diols **3b/c** requires contact with both ketoreductase enzymes, LbADH and Gre2p (see Supporting Figure 6). Therefore, the amount of **3b/c** is a quantitative indicator for migration of hydroxyketone intermediates between the fluid and gel phase. The graphs in (**B**) and (**C**) show the dependence of the diol formation on the concentration of the competing Gre2p enzyme in the liquid phase. Note that at equimolar concentrations of the active subunits of LbADH and Gre2p (50 µM each), (*R,R*)-products are predominantly formed (54%) along with 41% *meso*-products in the two phase system (**B**), while the mixture of unassembled enzymes (**C**) produces much higher amounts of the *meso*-product (58%) than of the (*R,R*)-product (37%). Error bars indicate the standard deviation, obtained from at least two independent experiments.

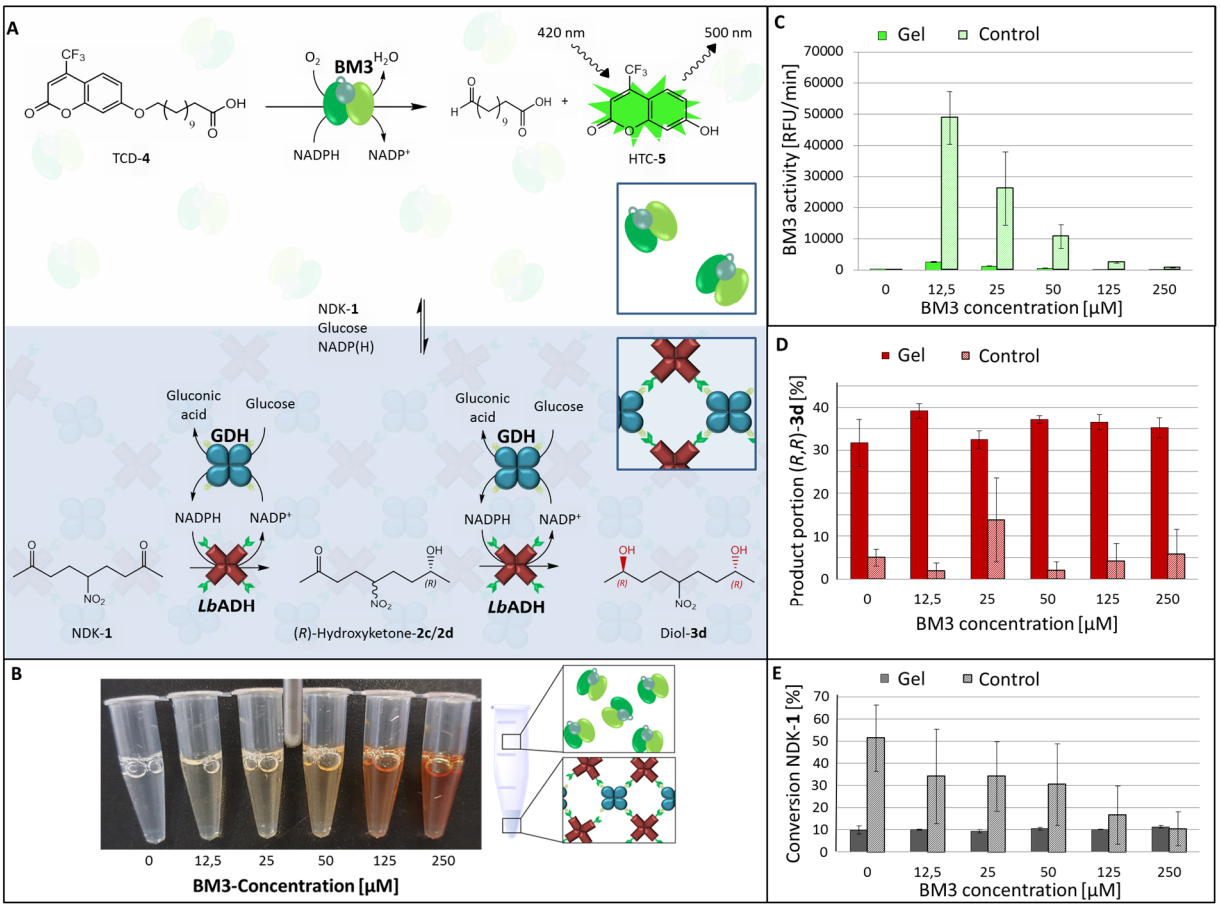

Supplementary Figure 10 | Compartmentalised competition assay with two enzymes competing for the same cofactor (NADPH) - Activity of the GDH-ST/SC-LbADH (50 µM subunits. each) gels and formation of diol product in the presence of variable P450 BM3 concentrations. (A) Similar as shown in Figure 2 (main text), the reaction scheme shows the competition of LbADH (red) and P450 BM3 (green) for NADPH as the cofactor of their respective reactions. The GDH (blue), which is located in the hydrogel, regenerates NADPH which is consumed by the LbADH (red) converting NDK-**1** while P450 BM3 (A74G, F87V)(green), which is located in the liquid bulk phase, is converting the fluorogenic TCD-**4** to HTC-**5**. (**B**) Photograph and schematic illustration of the clear hydrogel at the bottom of the reaction tube and the red coloured supernatant caused by the heme containing P450 BM3 in the liquid phase. The image was taken 150 min after addition of BM3. Note that the colourless gel indicates that no significant diffusion of BM3 occurs into the gel phase. (**C**) BM3 activity as determined by formation of fluorescent HTC-**5** in dependence on the BM3 concentration. Note that higher concentrations of P450 BM3 lead to quenching of the HTC-**5** fluorescence signal. Importantly, the activity in the control (light green bars) was 5-fold higher than in the the two-phase system gel (dark green bars) even at the highest concentration (250 µM) of P450 BM3. These results are indicative for compartmentalisation and entrapment of the NADP(H) with concomitant exclusion of the interfering P450 BM3. (**D**) Product portion of (*R*,*R*)-**3d** and (**E**) conversion of NDK-**1** in dependency of the BM3-concentration. Note that the productivity of the GDH-ST/SC-LbADH gels is substantially unaffected by increasing concentrations of the competing enzyme P450 BM3. All error bars indicate the standard deviation, obtained from at least two independent experiments.

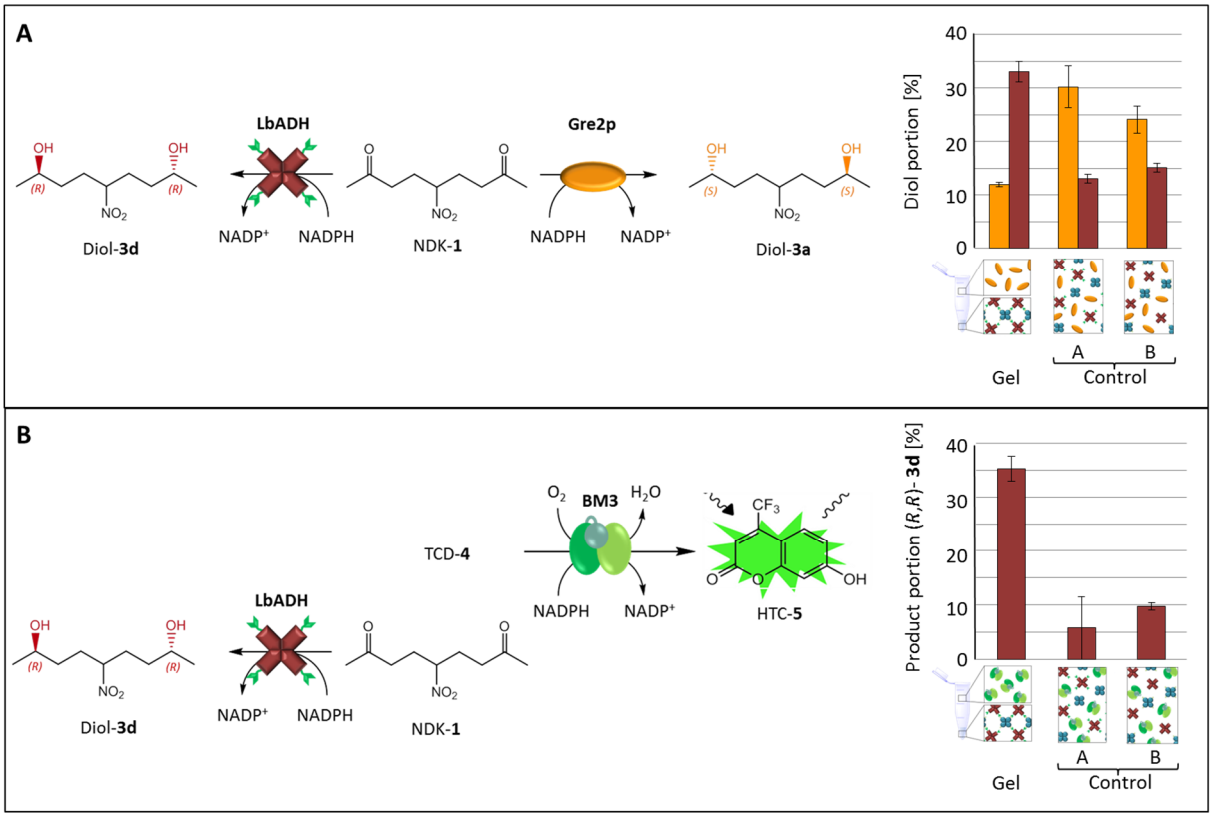

Supplementary Figure 11 | Different tagging of the control enzymes does not change the result of the compartmentalisation assay. (**A**) Reaction scheme of the compartmentalisation assay using 250 µM Gre2p as competitor (see also Figure 2). The product distribution clearly shows predominant formation of the (*R,R*)-**3d** diol by the GDH-ST/SC-LbADH hydrogel. In contrast, when the GDH/SC-LbADH (Control A) or GDH-ST/LbADH (Control B) are used as unassembled enzymes, the (*S,S*)-**3a** diol is predominantly formed, regardless of which enzyme is tagged with ST/SC. (**B**) Reaction scheme of the compartmentalisation assay with 250 µM P450 BM3 as competitor (similar as described in Supplementary Figure 10). Note that high amounts of product (*R,R*)-**3d** diol are produced by the GDH-ST/SC-LbADH hydrogel, whereas only small amounts of this diol are formed by unassembled GDH/SC-LbADH (Control A) or GDH-ST/LbADH (Control B), regardless of which enzyme is tagged with ST/SC. This result is indicative for compartmentalisation and sequestration of NADP(H) and hydroxyketones **2c/d** in the gel phase. Error bars indicate the standard deviation, obtained from at least two independent experiments.

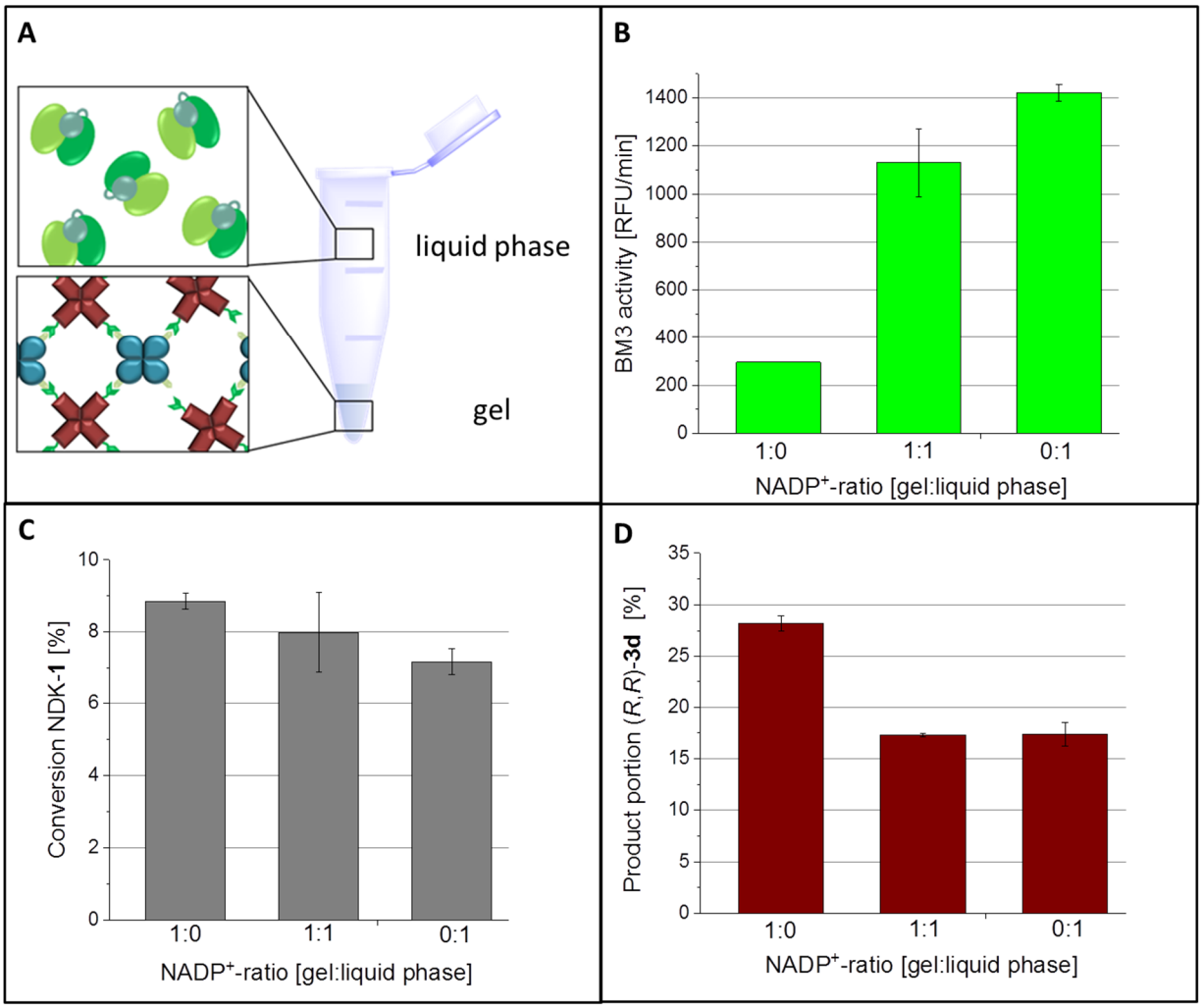

Supplementary Figure 12 | Activity of the GDH-ST/SC-LbADH hydrogel in the presence of P450 BM3 in the supernatant depending on the localisation of NADP$^+$. The cofactor NADP$^+$ was localised either in the gel (1:0), the liquid phase bulk solution (0:1) or equally distributed between the two phases (1:1) at the beginning of the reaction. (**A**) Schematic illustration of the compartmentalized competition assay containing GDH-ST/SC-LbADH hydrogel and P450 BM3 located in the supernatant. P450 BM3 converts TCD-**4** to the fluorescent HTC-**5**, as indicated in Supplementary Figure 11. (**B**) Highest conversion of **4** to **5** occurred when NADP$^+$ was localised in the liquid phase bulk solution (0:1). (**C**) Conversion of NDK-**1** to the (*R*)-configured hydroxyketones **2b/c** and (*R,R*)-**3d** diol products. Note that the localisation of NADP$^+$ has almost no influence on product formation. (**D**) Portion of (*R,R*)-**3d** diol products produced by the hydrogel. All product formations were determined after 2 h. Error bars indicate the standard deviation obtained from at least two independent experiments.

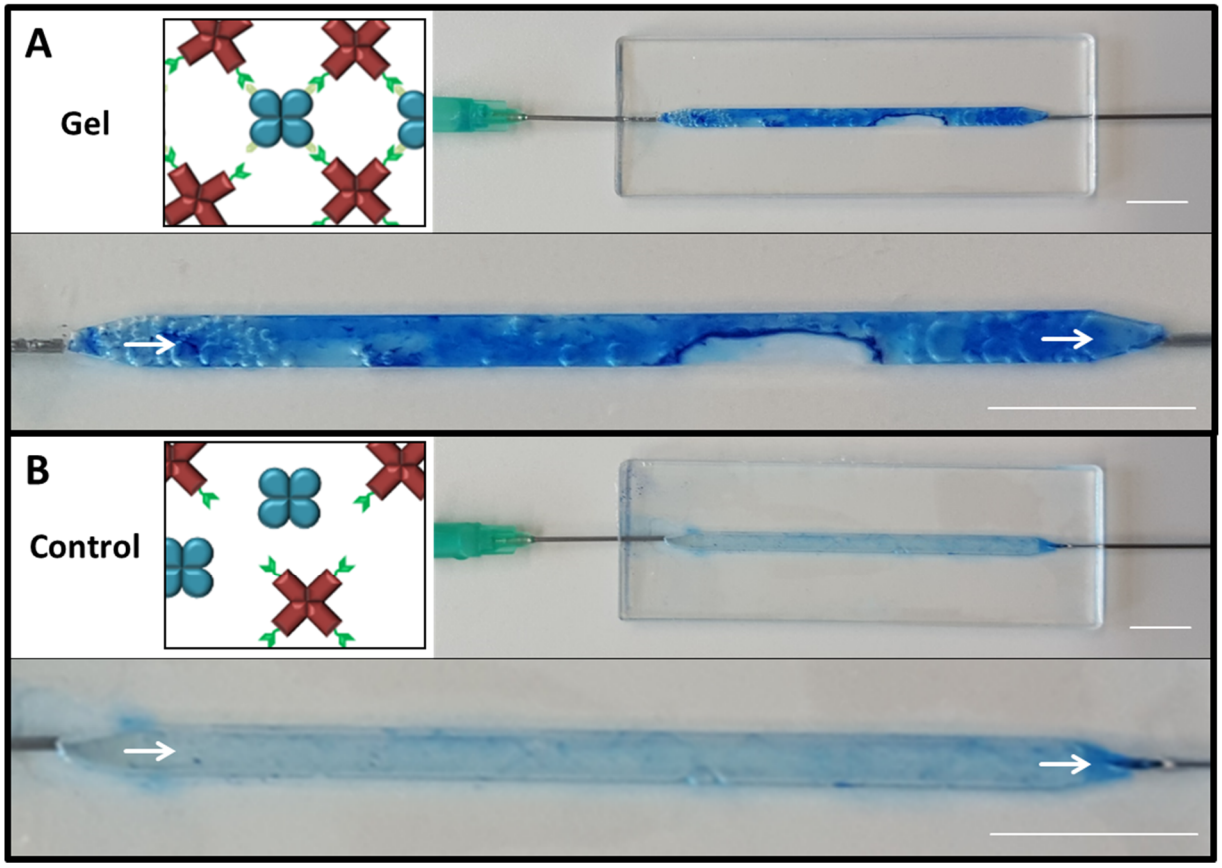

Supplementary Figure 13 | All-enzyme hydrogels can be used as stationary phase in microfluidic chips. The images show linear microfluidic chips (column volume (CV) = 150 µl) filled with the hydrogel (**A**) or unassembled enzymes as control (**B**) after running three hours at 10 µl/min and subsequent Coomassie staining of remaining proteins. Note that hydrogel immobilization and subsequent swelling led to encapsulation of air bubbles in the hydrogel, and perfusion with Coomassie solution did not lead to completely homogeneous staining of all areas of the channel. Scale bars are 1 cm.

Supplementary Tables

Supplementary Table 1 | Specific activities of the free enzymes using NDK-1 and glucose as substrates.

	MW	Homomeric subunits	Specific activity[a]	
	[$g_{protein}$/ $mol_{subunit}$]		[$\mu mol_{substrate}$/ (min*$mg_{protein}$)]	[$\mu mol_{substrate}$/ (min*$\mu mol_{subunit}$][b]
His-LbADH	27638	4	13.7 ± 0.8	380 ± 22
His-SC-LbADH	40080		6.6 ± 0,6	265 ± 24
GDH-His	29014		3.6 ± 0.4	104 ± 12
GDH-ST-His	31100		4.3 ± 0.4	133± 14
Gre2p-His	43333	1	1.4 ± 0.04	65 ± 2

[a] Specific activities of the enzymes using NDK-**1** and glucose as substrates. Data represent the mean of at least triplicate analyses ± 1 SD (standard deviation).

[b] Specific enzyme activity is normalized to protein subunits because Gre2p is a monomer [13] while LbADH[14] and GDH[15] are homotetramers.

References

1. Skoupi, M., Vaxelaire, C., Strohmann, C., Christmann, M. & Niemeyer, C.M. Enantiogroup-Differentiating Biocatalytic Reductions of Prochiral C -Symmetrical Dicarbonyl Compounds to meso Compounds. *Chem. Eur. J.* **21**, 8701-8705 (2015).
2. Gibson, D.G. et al. Enzymatic assembly of DNA molecules up to several hundred kilobases. *Nat Methods* **6**, 343-345 (2009).
3. Kossmann, K.J. et al. A Rationally Designed Connector for Assembly of Protein-Functionalized DNA Nanostructures. *Chembiochem* **17**, 1102-1106 (2016).
4. Peschke, T. et al. Self-Immobilizing Fusion Enzymes for Compartmentalized Biocatalysis. *ACS Catalysis* **7**, 7866-7872 (2017).
5. Peschke, T., Rabe, K.S. & Niemeyer, C.M. Orthogonal Surface Tags for Whole-Cell Biocatalysis. *Angew Chem Int Ed Engl* **56**, 2183-2186 (2017).
6. Kearse, M. et al. Geneious Basic: an integrated and extendable desktop software platform for the organization and analysis of sequence data. *Bioinformatics* **28**, 1647-1649 (2012).
7. Crocker, J.C. & Grier, D.G. Methods of digital video microscopy for colloidal studies. *Journal of Colloid and Interface Science* **179**, 298-310 (1996).
8. Vanhove, L. Correlations in Space and Time and Born Approximation Scattering in Systems of Interacting Particles. *Phys Rev* **95**, 249-262 (1954).
9. Weeks, E.R., Crocker, J.C., Levitt, A.C., Schofield, A. & Weitz, D.A. Three-dimensional direct imaging of structural relaxation near the colloidal glass transition. *Science* **287**, 627-631 (2000).
10. Hansen, S.H. et al. Machine-assisted cultivation and analysis of biofilms. *bioRxiv* (2017).
11. Zakeri, B. et al. Peptide tag forming a rapid covalent bond to a protein, through engineering a bacterial adhesin. *Proc. Natl. Acad. Sci.* **109**, E690-697 (2012).

12. Li, L., Fierer, J.O., Rapoport, T.A. & Howarth, M. Structural Analysis and Optimization of the Covalent Association between SpyCatcher and a Peptide Tag. *Journal of Molecular Biology* **426**, 309-317 (2014).
13. Breicha, K., Muller, M., Hummel, W. & Niefind, K. Crystallization and preliminary crystallographic analysis of Gre2p, an NADP(+)-dependent alcohol dehydrogenase from Saccharomyces cerevisiae. *Acta Crystallogr F* **66**, 838-841 (2010).
14. Leuchs, S. & Greiner, L. Alcohol Dehydrogenase from Lactobacillus brevis: A Versatile Robust Catalyst for Enantioselective Transformations. *Chem. Biochemi. Engin. Q.* **25**, 267-281 (2011).
15. Hilt, W., Pfleiderer, G. & Fortnagel, P. Glucose dehydrogenase from Bacillus subtilis expressed in Escherichia coli. I: Purification, characterization and comparison with glucose dehydrogenase from Bacillus megaterium. *Biochim Biophys Acta* **1076**, 298-304 (1991).